

Supplementary information

Legends to supplementary figures

Supplementary Figure 1: Homozygous deletion in *IFNAR1* in a patient who died from HSE and her cousin. (A) Brain MRI images showing HSE lesions. The parenchymal lesions display hazy enhancement on post-contrast T1 images (yellow arrows) (left). Temporoparietal edema with low apparent diffusion coefficient values, suggestive of a cytotoxic component (yellow triangles) (right). (B) Serological data for IgG antibodies against various viruses, for P2 at the age of 17 years, and his parents. The threshold value for each viral serological test is indicated. N: negative. P: positive. In serological tests for EBV, we measured anti-VCA antibody levels. (C) Antibody responses to microbial species for which at least one member of the family tested seropositive by VirScan. Species-specific score values for P2, his parents (III.3, III.4), 9 unrelated adult male blood donors (ABD), 2 unrelated adult healthy controls (AHC), 3 unrelated pediatric healthy controls (PHC), and pooled plasma used for intravenous immunoglobulin (IVIG) therapy, IgG-depleted serum and a mock IP sample (positive and negative controls). (D) Filtering criteria used for the single-nucleotide variant (SNV) analysis of whole-exome sequencing results for P1. MAF: minor allele frequency; CADD: combined annotation-dependent depletion; GDI: gene damage index. (E) Single nucleotide variants (SNVs) presented by the patient and meeting the filtering criteria, with the name, known function and expression pattern of the gene. (F) Whole-exome sequencing results for the *IFNAR1* gene in P1, as shown in ALAMUT, from exon 9 to 11. The region deleted in P1 is indicated with a red square.

Supplementary Figure 2: The *IFNAR1* deletion leads to aberrant splicing. (A) Alignment of the genomic regions flanking the *IFNAR1* deletion (intron 10 in orange, 3'UTR part of exon 11 in purple), with the 32 nt microhomology region in black. *AluSz* and *AluSc* sites are located in these regions. (B) Agarose gel electrophoresis of *IFNAR1* cDNA PCR products, amplified from PBMCs from P2, and a healthy control (Ctl) WT for IFNAR1. The result shown is representative of two independent experiments. (C) Schematic diagram of the amplified region of the *IFNAR1* cDNA in P2 and the control, showing the consequences of the deletion. The blue box indicates the 97 bp insertion in P2. The red box indicates the 473 bp deletion. The exons are numbered in roman numerals (X-XI). The new abnormal 'AG' splicing site, and the *AluSc* and *AluSz* regions are indicated.

Supplementary Figure 3: The mutant IFNAR1 protein does not bind TYK2. (A) Western blots (WB) of TYK2 and IFNAR1 after the co-immunoprecipitation of cell lysates of HEK293T cells cotransfected with WT or mutant *IFNAR1* cDNA constructs and WT TYK2. HEK293T cells were cotransfected with *TYK2* and various *IFNAR1* constructs for 48 h. Pulldown assays were performed with antibodies specific for TYK2. The bands correspondent to IFNAR1 are indicated with the blue asterisks. (B) WB of TYK2 and IFNAR1, without immunoprecipitation, for whole-cell lysates of HEK293T cells cotransfected with *TYK2* and various *IFNAR1* constructs for 48 h. The blots shown are representative of three independent experiments.

Supplementary Figure 4: Patient fibroblasts do not respond to IFN- α/β . (A) Extracellular FACS staining of IFNAR2 in SV40-fibroblasts from 3 healthy controls (C1, C2, C3), P2, and other patients (*IFNAR1*^{-/-}, *IFNAR2*^{-/-}, *IFNGR1*^{-/-}, *STAT1*^{-/-}). The cells were not permeabilized. An antibody recognizing the N-terminal (N-ter) part of the protein was used. Results representative of two independent experiments are shown. (B-D) Mean fluorescence intensity (MFI), after intracellular FACS staining of phosphorylated STAT1 (pSTAT1) (B), pSTAT2

(C) and pSTAT3 (D) in SV40-fibroblasts stimulated with 1,000 U/mL IFN- α 2b, IFN- β or IFN- γ for 15 min. The cells used were from three healthy controls (C1, C2, C3), P2, and IFNAR1^{-/-}, IFNAR2^{-/-}, IFNGR1^{-/-}, STAT1^{-/-}, and STAT2^{-/-} patients. The results shown are representative of three independent experiments. (E-H) MFI, after intracellular FACS staining of phosphorylated STAT1 (pSTAT1) (E), pSTAT2 (F) and pSTAT3 (G) in primary fibroblasts stimulated with 1,000 U/mL IFN- α 2b or IFN- γ for 15 min, and HLA-class I (H) induction after 48 h of stimulation with 1,000 U/mL IFN- α 2b or IFN- γ . The cells used were from three healthy controls (C1, C2, C3), P2, and IFNAR1^{-/-} and IFNGR1^{-/-} patients. The results shown are representative of two independent experiments. (I) WB of phosphorylated STAT1 (pSTAT1), pSTAT2, STAT1, STAT2 and IFNAR1, in P2 SV40-fibroblasts with and without transient transfection with WT or mutant IFNAR1 or an empty vector (EV), with and without stimulation with 1,000 U/mL IFN- α 2b for 15 min. GAPDH was used as a loading control. The results shown are representative of three independent experiments.

Supplementary Figure 5: Patient EBV-B cells do not respond to IFN- α / β . (A-C) Mean fluorescence intensity (MFI), after intracellular FACS staining of phosphorylated STAT1 (pSTAT1) (A), pSTAT2 (B) and pSTAT3 (C), in EBV-B cells stimulated with 1,000 U/mL IFN- α 2b, IFN- β , IFN- λ or IFN- γ for 15 min. The cells used were from four healthy controls (C1, C2, C3, C4), P2, and IFNAR1^{-/-}, IFNGR1^{-/-} and STAT1^{-/-} patients. The results shown are representative of three independent experiments.

Supplementary Figure 6: Abolished response to IFN- α / β in patient fibroblasts and rescue by exogenous WT IFNAR1 expression. (A) Heatmaps of RNA-seq-quantified gene expression (z -score scaling \log_2 read counts per million, cpm) showing the transcriptomic response to stimulation with IFN- α 2b (upper panels) or IFN- γ (lower panels) for two (left) or eight (right) hours, in primary fibroblasts from 3 healthy controls (C1, C2, C3), P2, the IFNAR1^{-/-} V225fs patient and an IFNGR1^{-/-} patient. Only genes with a $|\log_2(\text{FC})| > 1$ and a p -value < 0.05 relative to the control group are plotted. The blue to red gradient represents increasing z -scaled values. Hierarchical clustering was performed on samples and genes, on the basis of Euclidean distance values. (B) Scatter plots of $\log_2(\text{FC})$ in RNA-seq-quantified gene expression following stimulation with IFN- α 2b (top panels) or IFN- γ (bottom panels) for 2 (left panels) or 8 (right panels) hours, in primary fibroblasts from the IFNAR1^{-/-} V225fs patient versus three healthy controls (C1, C2 and C3). Each dot represents a single gene. (C) Levels of *MX1* and *IFIT1* mRNA, as measured by RT-qPCR, in SV40-fibroblasts from P2, with and without transient transfection with WT or mutant *IFNAR1* cDNA or EV, in the presence or absence of stimulation with IFN- α 2b or IFN- β for 2 or 8 h. *GUS* was used as an expression control. Mean and SD values from two independent experiments are shown.

Supplementary Figure 7: Enhanced viral replication in patient SV40-fibroblasts. (A) EV71 replication, quantified by the TCID₅₀ method, in SV40-fibroblasts from three healthy controls (C1, C2, C3), P2, and a previously published IFNAR1^{-/-} patient, 0, 10, 24, 48 and 72 h after infection with EV71 at a MOI of 10. (B) HSV-1 replication, quantified by the TCID₅₀ method, in SV40-fibroblasts from a healthy control (C1), and SV40-fibroblasts from P2 with and without stable transduction of WT IFNAR1 (WT), empty vector (EV) or a vector expressing GFP, 12, 24, and 48 h after infection with HSV-1 at a MOI of 0.01. The data shown are representative of two independent experiments. (C) WB of IFNAR1 in SV40-fibroblasts from C1, and from P2, with and without stable transduction of WT IFNAR1, EV or a vector expressing GFP. An antibody recognizing the N-terminal side of the protein was used. GAPDH was used as a loading control.

Patient clinical history

We studied a girl (P1), born to parents from a consanguineous kindred of Arab origin. She was healthy and developed normally until the age of 13 months, when she developed a prolonged fever. She was eventually diagnosed with atypical Kawasaki disease, without typical cardiac involvement. She was hospitalized for 30 days, received intravenous immunoglobulin (IVIG) therapy twice and recovered. At the age of 16 months, she was again hospitalized for gingivostomatitis and aseptic meningitis. She recovered after 30 days of treatment with broad-spectrum antibiotics, acyclovir and blood transfusions. She was also treated with IVIG and pulse steroid therapy, due to neurological symptoms and suspected bulbar palsy. At the age of 19 months, she was readmitted to a local hospital after a week of fever and oral lesions accompanied by focal seizures. HSV-1 PCR on cerebrospinal fluid (CSF) was positive. Brain electroencephalography showed signs of epilepsy in the left temporal lobe and brain magnetic resonance imaging revealed lesions in the left parietal lobe and left temporal-occipital lobe (Figure 1B, S Figure 1A). P1 was diagnosed with herpes simplex encephalitis and treated with intravenous acyclovir, but she remained semi-conscious. She was transferred to a larger medical center, where she was treated for one month. Despite intravenous acyclovir treatment, HSV-1 PCR on CSF continued to yield positive results and the patient remained in a semi-conscious state. Upon discharge, no hand or leg movement was detected. The patient died one month later, due to the severe neurological syndrome.

A cousin (P2) from the same family had suffered two episodes of “aseptic” meningitis at the ages of six and 10 months. Herpes simplex virus (HSV) infection was suspected, but PCR was not performed. P2 was treated empirically with acyclovir and recovered fully. At the age of 14 years, he developed parotitis, which was followed by bilateral hearing loss necessitating cochlear implants. Mumps virus infection was thought to be responsible for this episode, and this patient was tested positive for anti-mumps IgG antibody at the age of 17 years (S Figure 1B). The patient is now 17 years old and has developed no other severe infections. Viral serological data showed him to be positive for antibodies against various viruses, including HSV-1, human herpes viruses 4, 5, and 6, rhinovirus, adenovirus, enterovirus B, varicella zoster virus (VZV), cytomegalovirus, Epstein-Barr virus, measles virus, mumps virus, hepatitis A virus, influenza A virus and respiratory syncytial virus (S Figure 1B,C).

Another cousin of P1 (P3, a sibling of P2) died following a severe adverse reaction to MMR vaccination at 12 months of age. No biological material was available for P3 and it was not possible to perform a genetic study for this patient. No severe diseases were reported in other family members. P1 was fully vaccinated against hepatitis B virus, poliovirus, diphtheria, tetanus and whooping cough, type B *Hemophilus influenzae* and pneumococcus, and MMR. Following MMR vaccination, she developed a high fever that resolved spontaneously. A sister of P1 was born preterm, at 30 weeks of gestation, and died from complications of prematurity. The other children of this large kindred, including P2, did not receive MMR vaccine, in accordance with the parents’ wishes, due to the death of P3 following MMR vaccination.

Whole-exome sequencing

Exome capture was performed with the SureSelect Human All Exon 50 Mb kit (Agilent Technologies). Paired-end sequencing was performed on a HiSeq 2000 (Illumina) generating 100-base reads. We aligned the sequences with the GRCh37 reference build of the human genome with the BWA (1). Downstream processing and variant calling were performed with the Genome Analysis Toolkit, SAMtools, and Picard (2, 3). Substitution and InDel calls were made with GATK Unified Genotyper. All variants were annotated with an annotation software system developed in-house (4–6).

RNA-sequencing analysis

The RNA-seq fastq files were first inspected with FastQC (<https://www.bioinformatics.babraham.ac.uk/projects/fastqc/>) to ensure that the raw data were of high quality. For each subject, the four fastq files generated were then mapped to the human reference genome (Ensembl GRCh37 release 75) with STAR v.2.7.3a in the two-pass mode (7). The mapping quality of each bam file was then evaluated with RSeQC (8). Reads were quantified to generate gene-level feature counts from the read mapping, with HTSeq-count v.0.11.2 (9). We retained only protein-coding genes for further analyses and filtered out genes with low levels of expression with the filterByExpr function implemented in the edgeR package with default parameters other than min.total.count, which was set to 300. We accounted for differences in read counts at the tails of the distribution, by normalizing each sample with the weighted trimmed mean of M-values algorithm (TMM), as implemented in edgeR. We then log-transformed the data with the voom function implemented in the limma package v3.42.2 (10). We then fitted these log-transformed expression estimates to a linear model with a factor for phenotype group (healthy controls, IRF1 patient (P2), IFNAR1^{-/-} patient, and IFNGR1^{-/-} patient), treatment conditions (non-stimulated, stimulation with IFN- α 2b, stimulation with IFN- γ) and duration of treatment (two hours, eight hours), using the lmFit function implemented in the limma package, and estimated differential gene expression effects. For each phenotype group, we thus compared the samples stimulated with IFN- α 2b or IFN- γ for two or eight hours with the non-stimulated samples. For the group of three healthy controls, differentially expressed genes were defined as those with P values ≤ 0.05 after Benjamini-Hochberg correction, and a $|\log_2(\text{FC})| \geq 1$. Differential gene expression was plotted in heatmaps with pheatmap v1.0.12. Hierarchical clustering was performed on Euclidean distances, for genes and samples, according to the complete linkage method.

Phage Immunoprecipitation-Sequencing

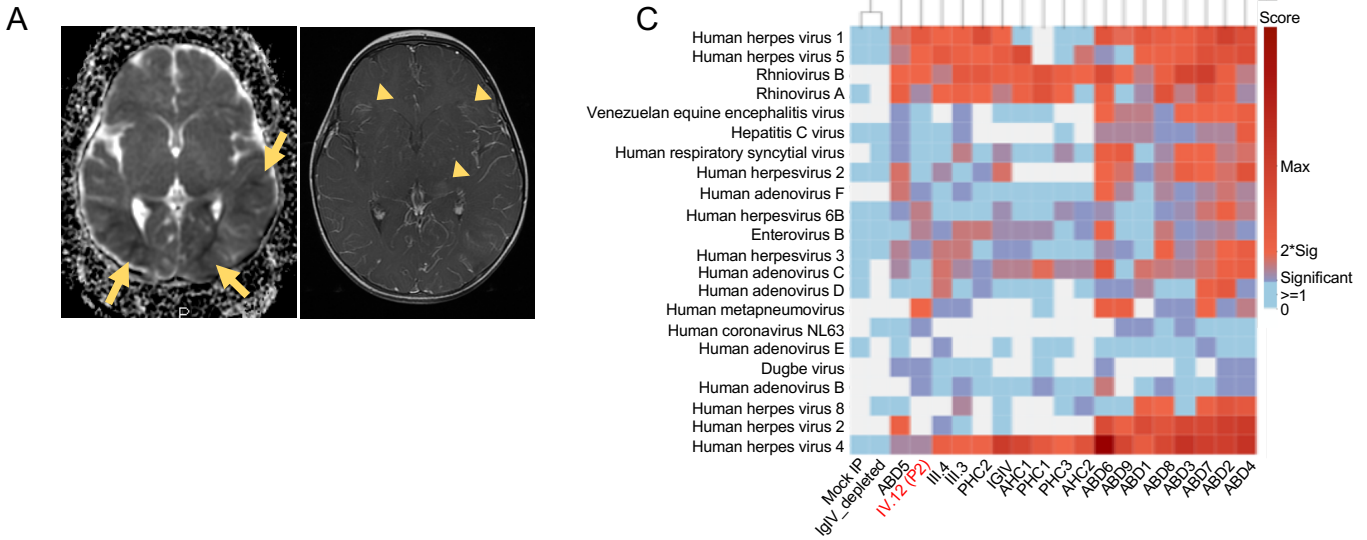
Phage Immunoprecipitation-Sequencing (PhIP-Seq) was performed as described previously (11–14) and analyzed with the following modifications. We computed species-specific significance cut-off values to estimate minimum number of enriched, non-homologous peptides required in order to consider a sample as seropositive using generalized linear model and in-house data generated from a large number of donors ($n = 800$). We then computed virus score values as described by Xu et al (13) scores by counting enriched, non-homologous peptides for a given species and then adjusted these score values by dividing them with the estimated score cutoff. These adjusted virus scores (Virus Score_{adj}) were depicted in heatmap plots and used for principal component analysis. For comparison, we analyzed the patient's and his parents' antibody profile along with nine randomly selected adult male blood donor of various nationality and Arab ancestry, three healthy adolescent females who had received Gradasil, as well as two additional unrelated adult controls. Pooled human plasma used for IVIg (Privigen® CSL Behring AG) and human IgG-depleted serum (Molecular Innovations, Inc.) served as additional controls. Human subject research related to the antibody profiling was approved by the Institutional Research Ethics Boards of Sidra Medicine.

References

1. Li H, Durbin R. Fast and accurate short read alignment with Burrows-Wheeler transform. *Bioinformatics* 2009;25(14):1754–1760.
2. Li H et al. The Sequence Alignment/Map format and SAMtools. *Bioinformatics* 2009;25(16):2078–2079.
3. McKenna A et al. The Genome Analysis Toolkit: A MapReduce framework for analyzing next-generation DNA sequencing data. *Genome Res* 2010;20(9):1297–1303.
4. Ng PC, Henikoff S. Predicting deleterious amino acid substitutions. *Genome Res* 2001;11(5):863–874.

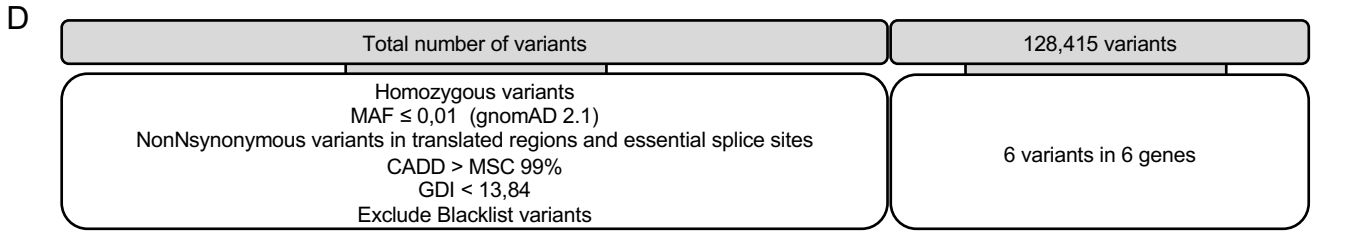
5. Kircher M et al. A general framework for estimating the relative pathogenicity of human genetic variants. *Nat. Genet.* 2014;46(3):310–315.
6. Adzhubei IA et al. A method and server for predicting damaging missense mutations. *Nat. Methods* 2010;7(4):248–249.
7. Dobin A et al. STAR: ultrafast universal RNA-seq aligner. *Bioinformatics* 2013;29(1):15–21.
8. Wang L, Wang S, Li W. RSeQC: quality control of RNA-seq experiments. *Bioinformatics* 2012;28(16):2184–2185.
9. Anders S, Pyl PT, Huber W. HTSeq--a Python framework to work with high-throughput sequencing data. *Bioinformatics* 2015;31(2):166–169.
10. Ritchie ME et al. limma powers differential expression analyses for RNA-sequencing and microarray studies. *Nucleic Acids Res.* 2015;43(7):e47.
11. Drutman SB et al. Fatal Cytomegalovirus Infection in an Adult with Inherited NOS2 Deficiency. *N. Engl. J. Med.* 2020;382(5):437–445.
12. Kerner G et al. Inherited human IFN- γ deficiency underlies mycobacterial disease. *J. Clin. Invest.* 2020;130(6):3158–3171.
13. Xu GJ et al. Viral immunology. Comprehensive serological profiling of human populations using a synthetic human virome. *Science* 2015;348(6239):aaa0698.
14. Mohan D et al. Publisher Correction: PhIP-Seq characterization of serum antibodies using oligonucleotide-encoded peptidomes. *Nat Protoc* 2019;14(8):2596.

Supplementary Figure 1



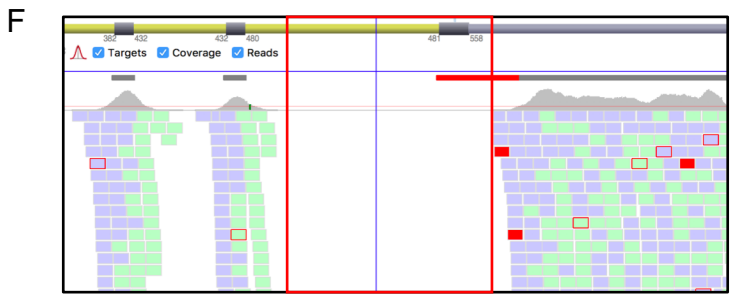
B

	HSVN1	HSVN2	VZV	CMV	EBV (IgG VCA)	Measles	Rubella	Mumps	HAV	Parvovirus B19	IAV	IBV	VRS
III.3	51	N	2673	170	472	>300	231	N	P	N	32	N	32
III.4	35	N	1931	> 180	> 600	>300	>350	286	P	N	N	N	32
IV.12 (P2)	20	N	239	124	121	>300	N	>300	P	N	16	N	8
Threshold	1,1	1	165	12	20	16,5	10	11		1,1	4	4	4



E

Gene	Gene name	Gene function	Expression	AAChange	Function	CADD	Zygo
ACSF3	acylCoA synthetase family member 3	Activate fatty acids by catalyzing the formation of a thioester linkage between fatty acids and coenzyme A	Broad	p.Thr67Met	missense	26,5	hom
KIAA0513	KIAA0513	Unknown, could interact with with modulators of neuroplasticity, apoptosis, and the cytoskeleton	Brain	p.Pro199Leu	missense	10,13	hom
KRTAP10N11	keratin associated protein 10N11	Unknown	Unknown	p.Pro134Thr	missense	15,2	hom
LOXL1	lysyl oxidase like 1	biogenesis of connective tissue	heart, prostate	p.Pro266dup	IndelInframe	9,47	hom
NCOR2	nuclear receptor corepressor 2	Nuclear receptor coNrepressor that mediates transcriptional silencing of certain target genes	fat, lung, broad	p.Glu524Gly	missense	24,3	hom
TRIM40	tripartite motif containing 40	May play a role as a negative regulator against inflammation and carcinogenesis in the gastrointestinal tract	Digestive tract	p.Met185Val	missense	2,31	hom

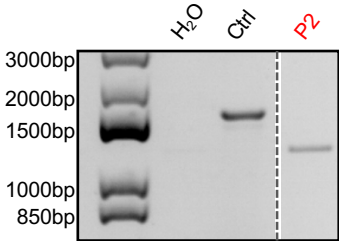


Supplementary Figure 2

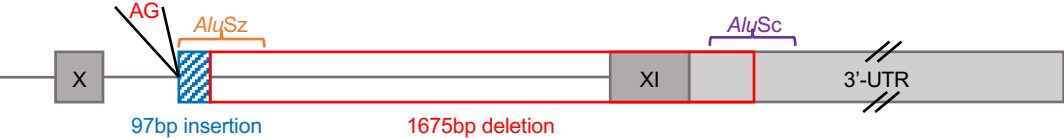
A

Intron 10 (WT)	GGCCAAGCGTGGTGGCTCAGCCTGTAAATCCAGCACTTTGGGAGGCTGAGGC	GGGTGGG	<i>AluSz</i>
MT	GGCCAAGCGTGGTGGCTCAGCCTGTAAATCCAGCACTTTGGGAGGCTGAGGC	AGGCAGA	
3' UTR Exon 11 (WT)	--CCGGGCACGGTGGCTCACACCTGTAAATCCAGCACTTTGGGAGGCTGAGGC	AGGCAGA	<i>AluSc</i>
Intron 10 (WT)	TCACCTTGAGTTCAGGAGTTCGAGACCAGCCTGGTCAACATGGAGAAACCCCTGTCTCTACT		<i>AluSz</i>
MT	TCA--TGAGTCAAGAGATCGAGACCAGCCTGGCCACGTGGTGAACCCCATCTCTACT		
3' UTR Exon 11 (WT)	TCA--TGAGTCAAGAGATCGAGACCAGCCTGGCCACGTGGTGAACCCCATCTCTACT		<i>AluSc</i>
Intron 10 (WT)	AAAAATATAAAA--TTAGCCGGGCGTGGTGGCACAATGCCTGTAAATCCAGCTACTCGGGAG		<i>AluSz</i>
MT	AAAAATACAAAAATTAGCCGGGCGTGGTGGCAGCGCCCTGTGTCTTAGCTACTCAGGAG		
3' UTR Exon 11 (WT)	AAAAATACAAAAATTAGCCGGGCGTGGTGGCAGCGCCCTGTGTCTTAGCTACTCAGGAG		<i>AluSc</i>
Intron 10 (WT)	GCTGAGGCAGGAGAATCGCTTGAAAAACAGGAGGTGGAGGTTGCAGTGAGCCGAGATCAGC		<i>AluSz</i>
MT	GCTGAGGCAGGAGAATCGCTTGAAAAACAGGAGGTGGAGGTTGCAGTGAGCCGAGATCAGC		
3' UTR Exon 11 (WT)	GCTGAGGCAGGGGATCGCTTGAACCTGGGAGGTGGAGGTTGCAGTGAGCCGAGGTCATG		<i>AluSc</i>
Intron 10 (WT)	CCACTGCACCTCCAGCCTGGGTGACAGAGCAAGACTCTGTCTCTAAATAAGTAAATAAA		<i>AluSz</i>
MT	CCACTGCACCTCCAGCCTGG--TGACAGCGTGAGACTCT----TTAAAAAAGAAA----		
3' UTR Exon 11 (WT)	CCACTGCACCTCCAGCCTGG--TGACAGCGTGAGACTCT----TTAAAAAAGAAA----		<i>AluSc</i>

B



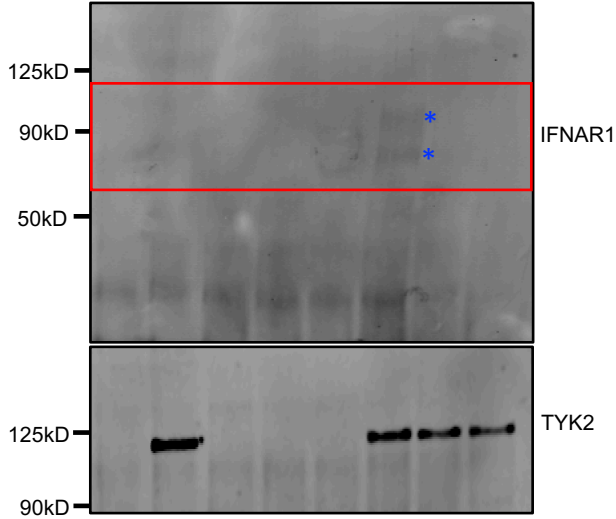
C



Supplementary Figure 3

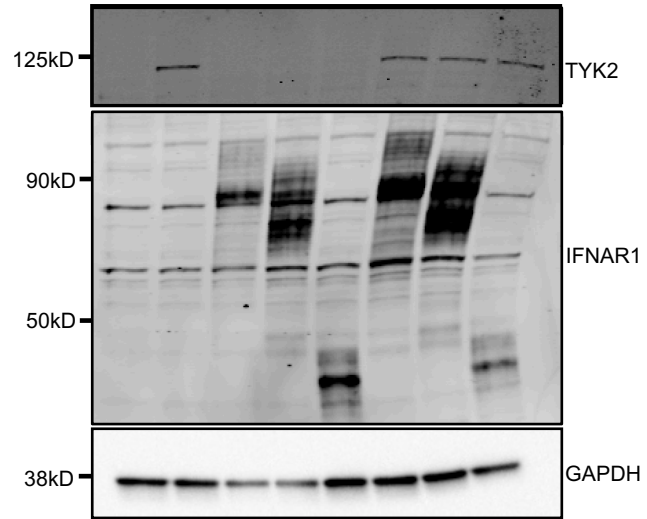
A Pulldown with TYK2 Ab

	EV	+	+	+	+	-	-	-
EV	+	+	+	+	+	-	-	-
TYK2	-	+	-	-	-	+	+	+
IFNAR1 WT	-	-	+	-	-	+	-	-
IFNAR1 MT	-	-	-	+	-	-	+	-
IFNAR1 V225fs	-	-	-	-	+	-	-	+

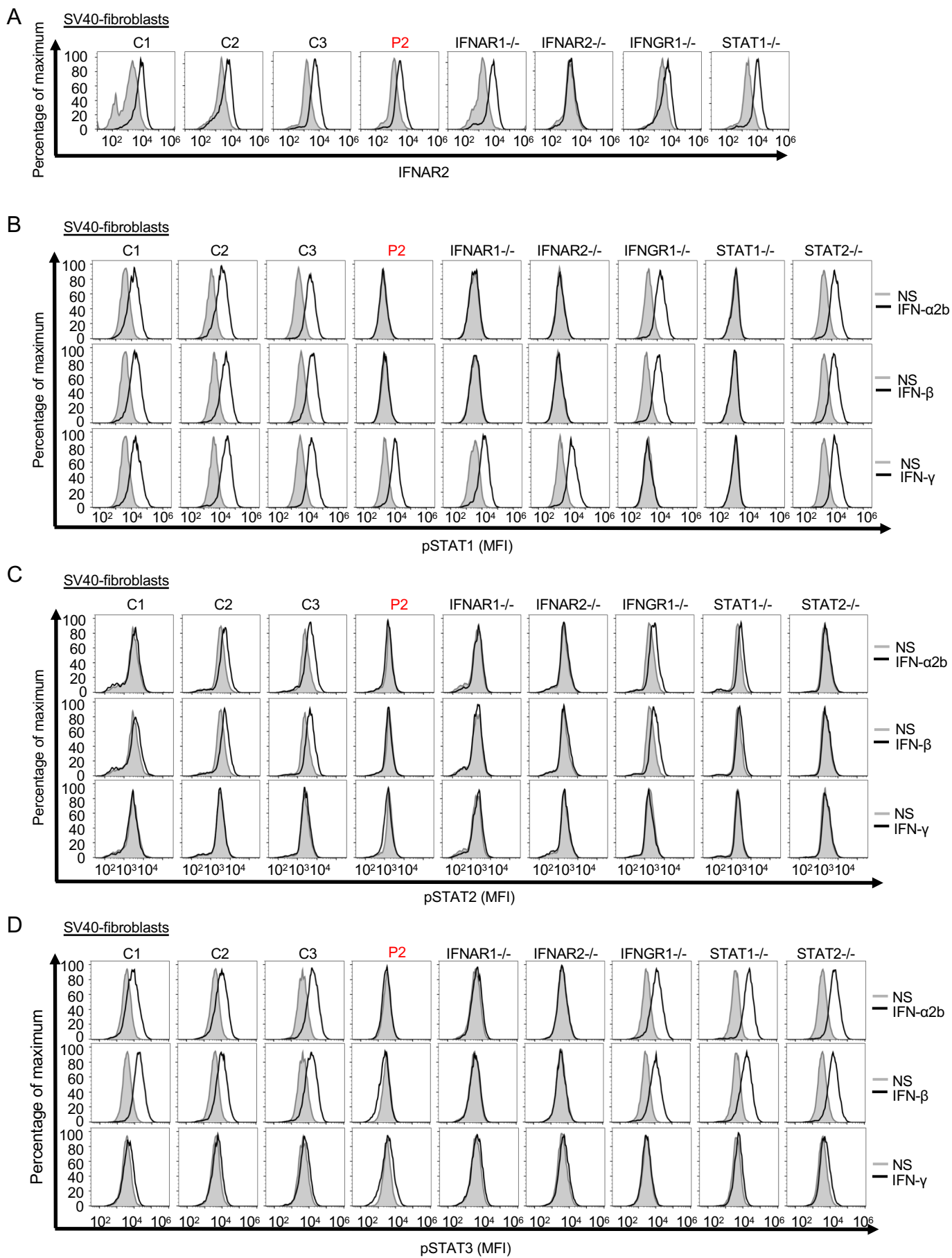


B Whole protein fraction

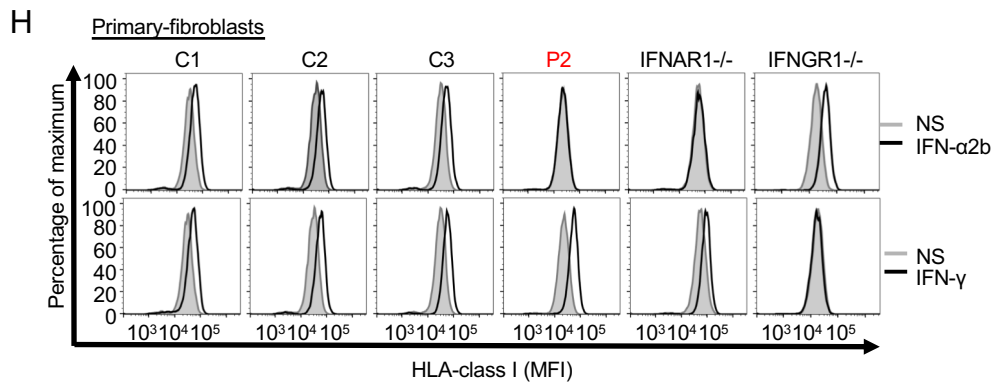
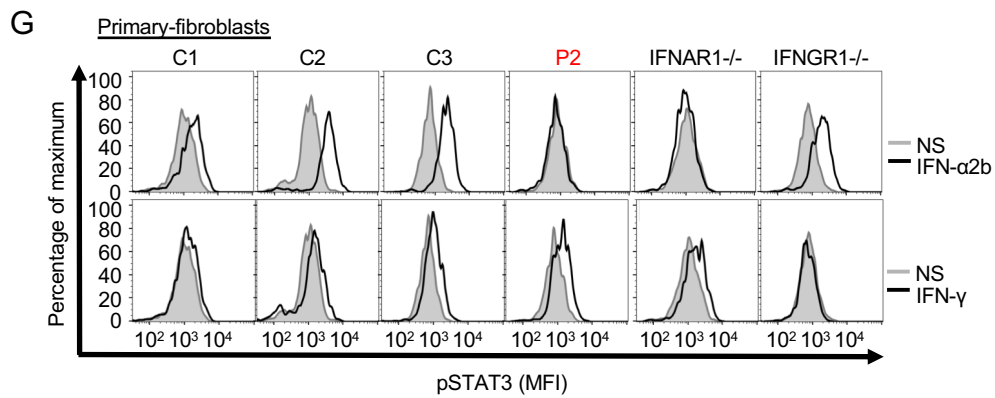
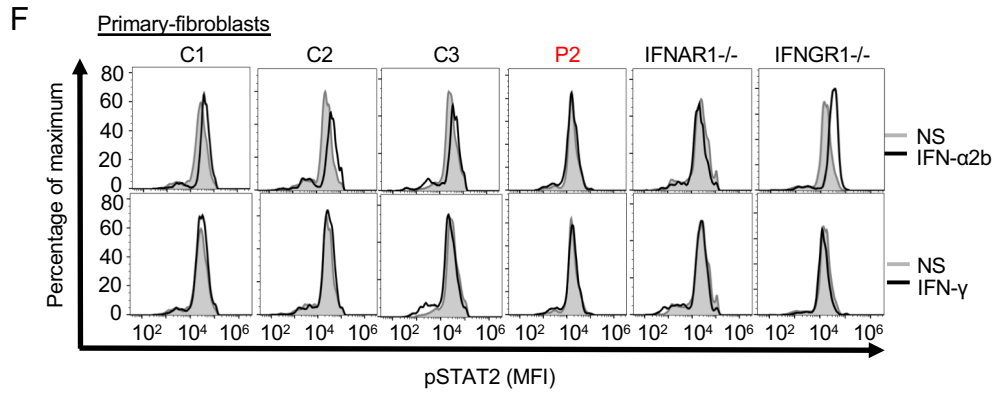
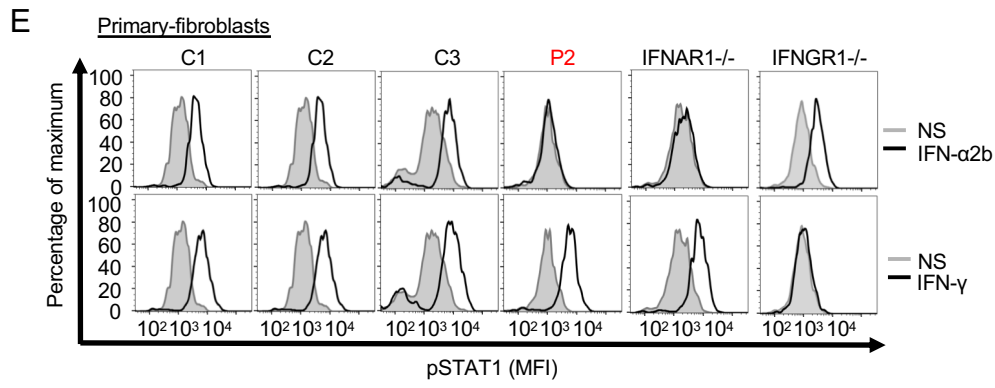
	EV	+	+	+	+	-	-	-
EV	+	+	+	+	+	-	-	-
TYK2	-	+	-	-	-	+	+	+
IFNAR1 WT	-	-	+	-	-	+	-	-
IFNAR1 MT	-	-	-	+	-	-	+	-
IFNAR1 V225fs	-	-	-	-	+	-	-	+



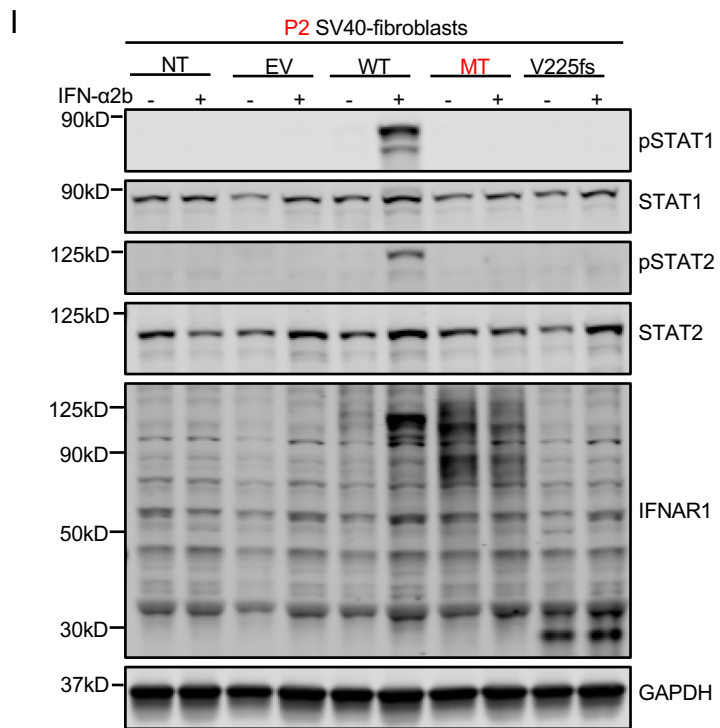
Supplementary Figure 4



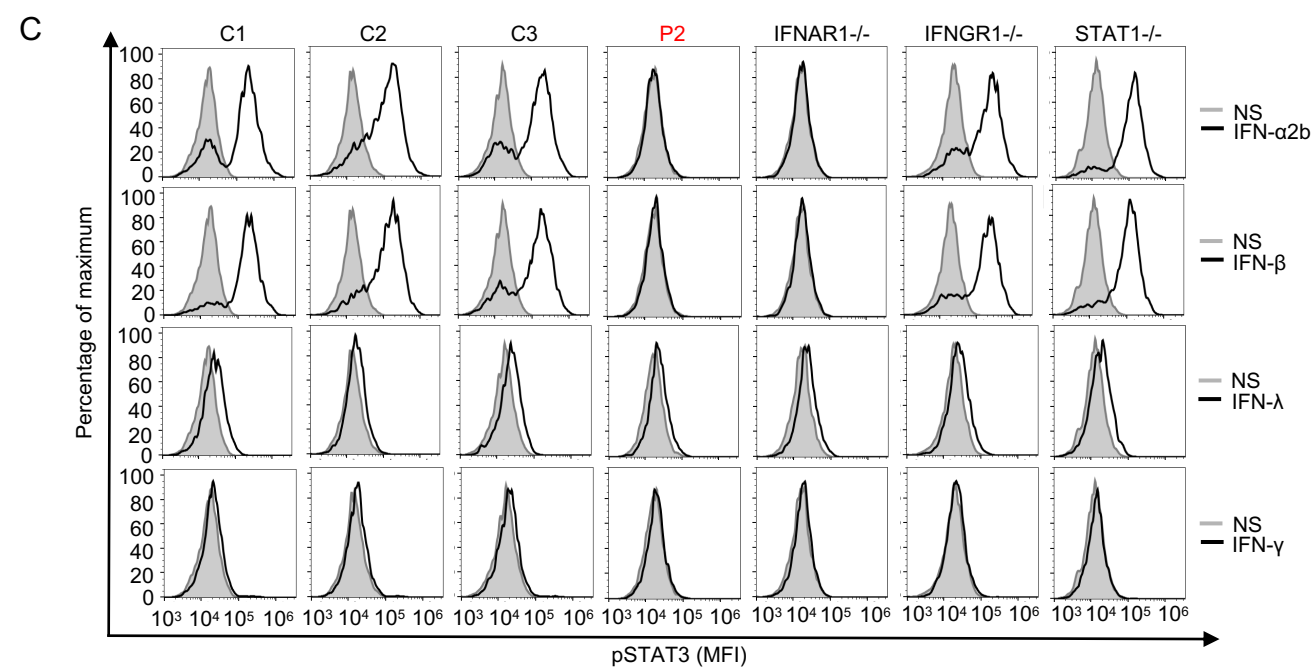
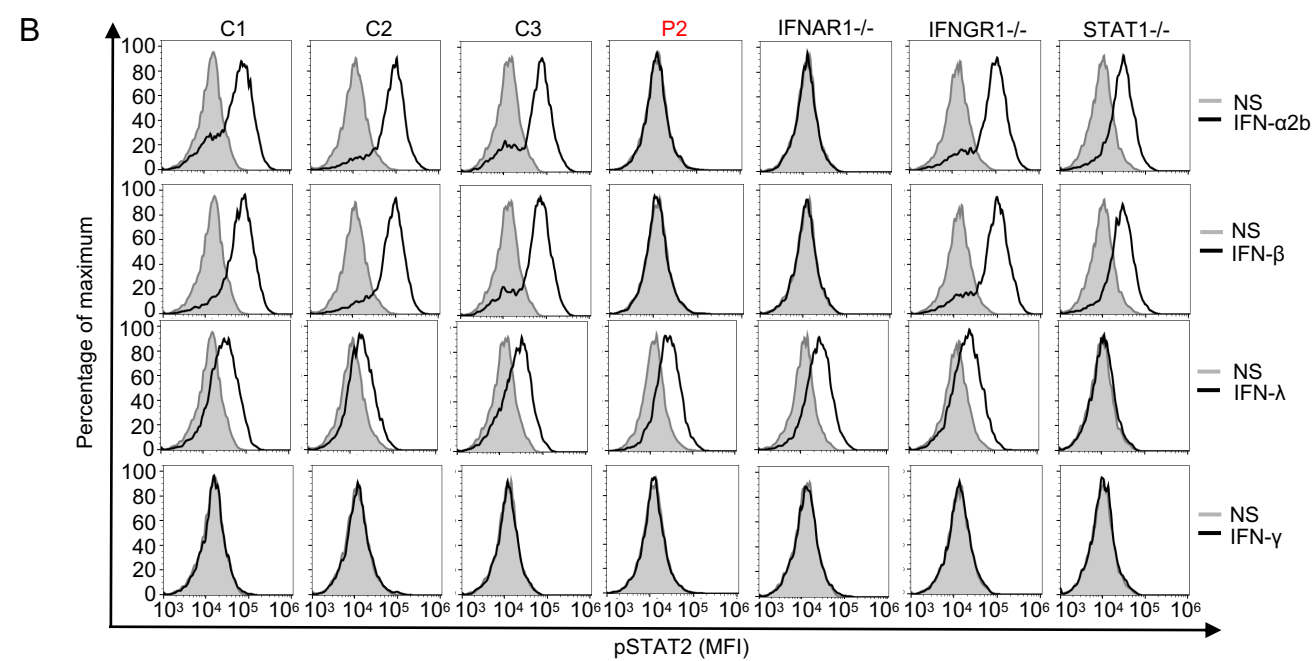
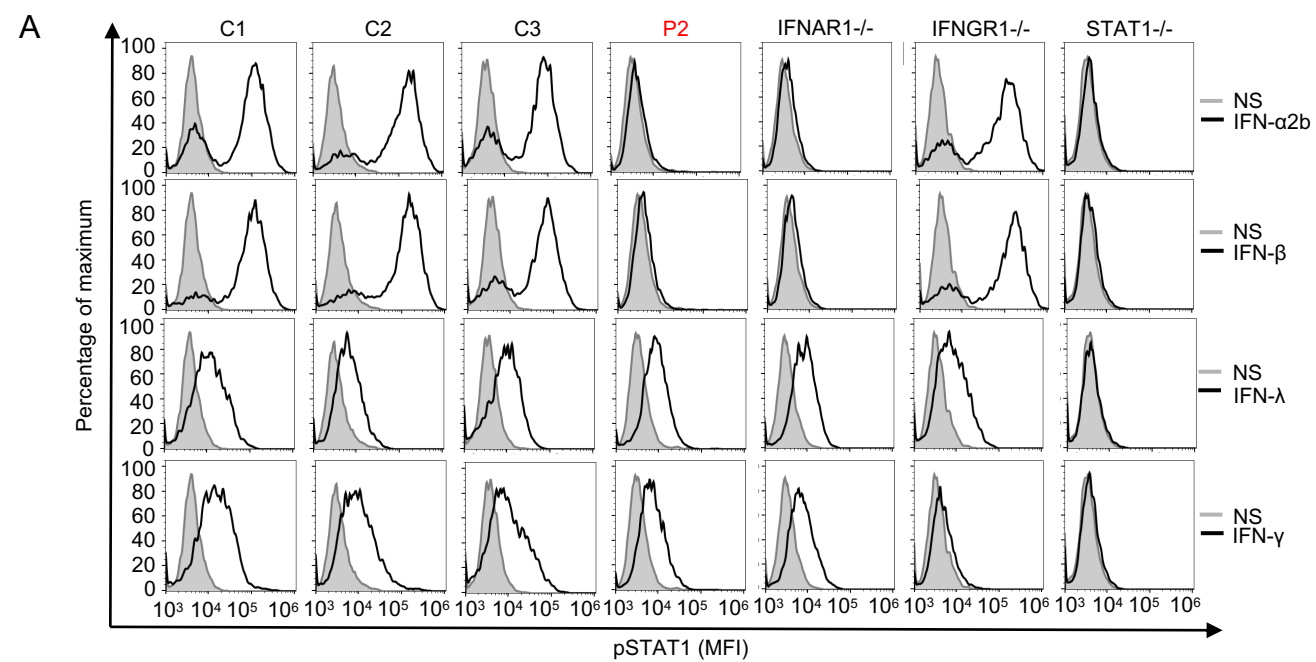
Supplementary Figure 4



Supplementary Figure 4

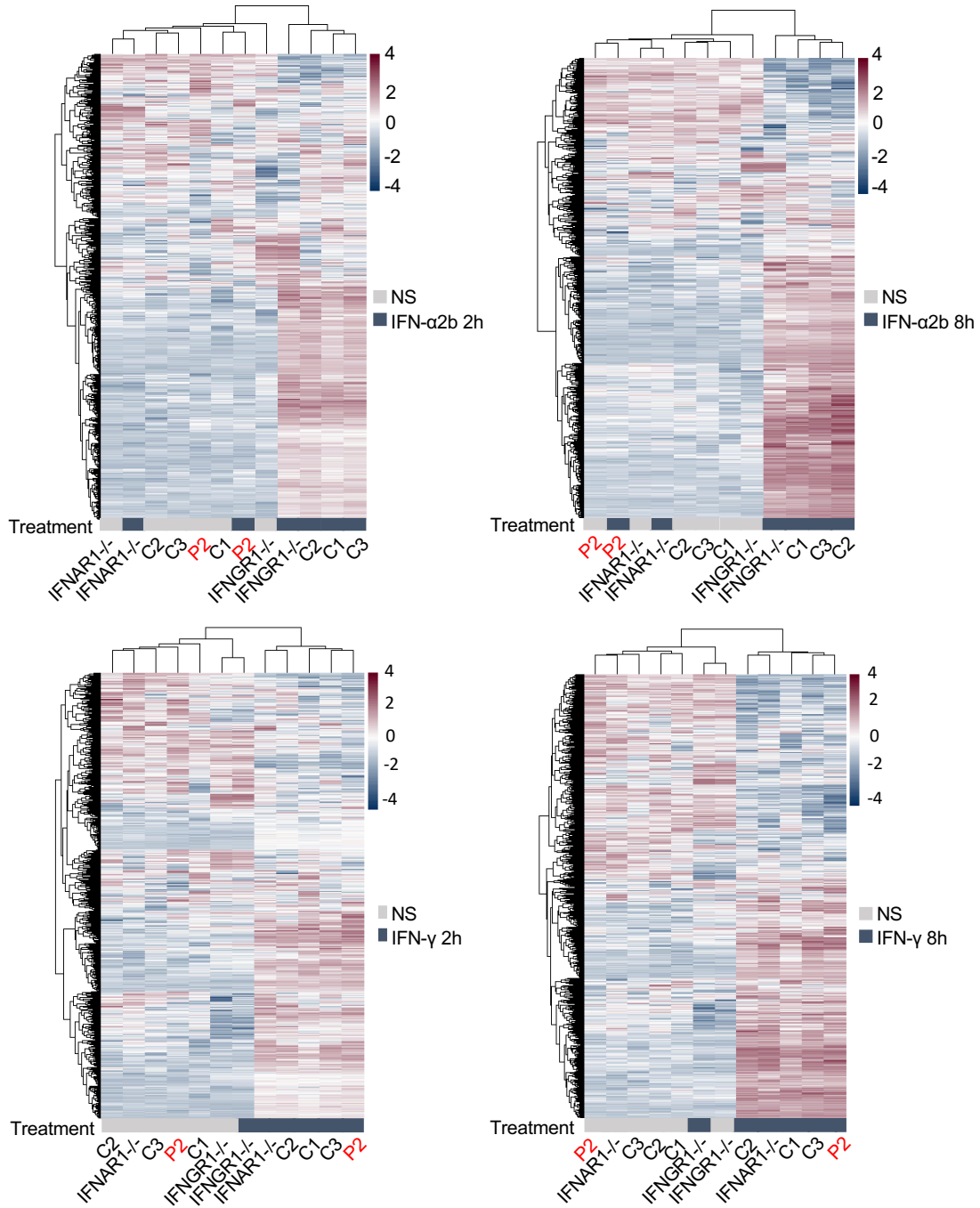


Supplementary Figure 5

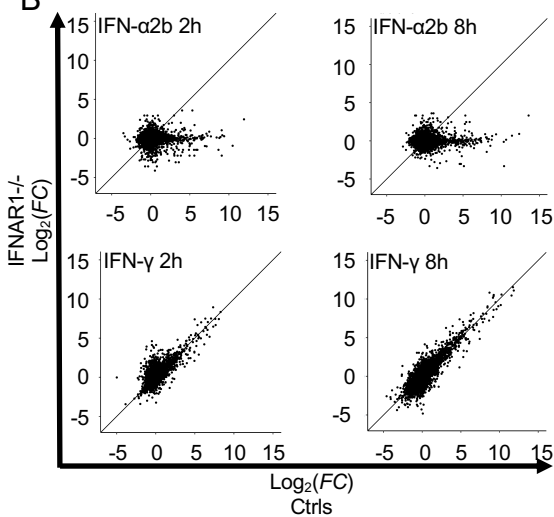


Supplementary Figure 6

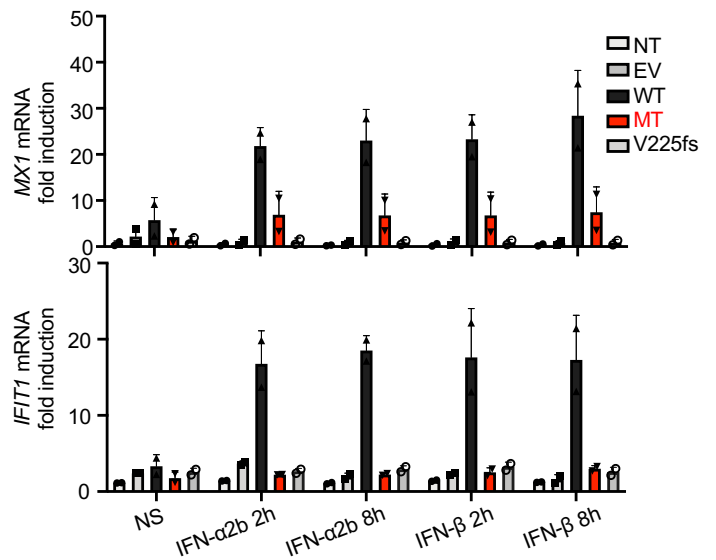
A



B



C



Supplementary Figure 7

